

## Nuclear Reactions of Cobalt with Protons from 0- to 100-Mev Energy\*

RODMAN A. SHARP,<sup>†</sup> RICHARD M. DIAMOND,<sup>‡</sup> AND GEOFFREY WILKINSON<sup>§</sup>  
*Department of Chemistry, Harvard University, Cambridge, Massachusetts*

(Received August 9, 1955)

Absolute excitation functions for 0- to 100-Mev protons on cobalt have been measured for 18 radioactive products from vanadium through nickel. Linear-accelerator bombardments in the 0- to 30-Mev region plus a scattered-beam cyclotron technique gave good energy resolution. The results are in qualitative agreement with the Bohr compound nucleus picture at low energies and a mixture of the Bohr and Serber mechanisms at higher energies. Evidence for high yields of alpha-particle emission was found. The influence of shell structure on yields was pronounced, with magic-number nuclei having especially low yields.

### I. INTRODUCTION

**R**ADIOCHEMICAL yield studies are of interest particularly for the opportunities they provide for comparison with current theories of nuclear reactions and nuclear structure. Excitation function studies provide an energy variable in addition to the atomic number and weight parameters found in most spallation experiments. In view of the present condition of theories of nuclear behavior, it is desirable to pick a simple system to study. For this reason, cobalt, a monoisotopic target element of medium atomic weight was chosen for proton irradiation. The energy range of 0-100 Mev for simple reactions bridges the region usually treated by compound nucleus theory and the higher energy ranges where nuclear transparency becomes important.

A number of papers have appeared recently on the proton spallation of cobalt. In an extensive survey, Belmont and Miller<sup>1</sup> reported absolute yields of 35 nuclides from carbon through nickel using 370-Mev protons. Wagner and Wiig<sup>2</sup> reported relative yields for 14 products from 240-Mev proton bombardment, and in a later paper gave absolute yields at 60, 100, 170, and 240 Mev for nine of the species previously measured at 240 Mev.<sup>3</sup> In connection with a spallation survey covering several targets, Rudstam<sup>4</sup> gave yields for eleven nuclides relative to Cr<sup>49</sup> for 187-Mev protons on cobalt.

### II. EXPERIMENTAL<sup>5</sup>

#### A. Targets

The targets used in these experiments were thin cobalt foils of 8-120 mg/cm<sup>2</sup> thickness. They were

\* This work was supported in part by the U. S. Atomic Energy Commission.

<sup>†</sup> Present address: Chemistry Department, Brookhaven National Laboratory, Upton, Long Island, New York.

<sup>‡</sup> Present address: Chemistry Department, Cornell University, Ithaca, New York.

<sup>§</sup> Present address: Chemistry Department, Imperial College of Science and Technology, London, England.

<sup>1</sup> E. Belmont and J. M. Miller, *Phys. Rev.* **95**, 1554 (1954).

<sup>2</sup> G. D. Wagner and E. O. Wiig, *J. Am. Chem. Soc.* **74**, 1101 (1952).

<sup>3</sup> G. D. Wagner and E. O. Wiig, *Phys. Rev.* **96**, 1100 (1954).

<sup>4</sup> S. G. Rudstam, *Phil. Mag. Ser. 7*, **44**, 1131 (1953).

<sup>5</sup> Additional details may be found in the Ph.D. thesis of Rodman A. Sharp, Harvard University, 1955 (unpublished).

produced electrolytically by a method similar to that of Sisman and Bopp.<sup>6</sup> A bath consisting of 0.7M CoSO<sub>4</sub> and 0.7M H<sub>3</sub>BO<sub>3</sub> was electrolyzed between a platinum anode and a stainless steel cathode at a current density of 40 ma/cm<sup>2</sup>. The cathode surface was abraded with No. 80 emery paper before plating to insure adhesion. Flexible hole-free foils were produced at the rate of 20 mg/cm<sup>2</sup> hr and after a few seconds dip in aqua regia to remove the highly active surface layer, they remained bright indefinitely.

The best analytical-reagent grade cobalt salts available (Mallinckrodt Chemical Company) were guaranteed 99.6% pure with 0.15% nickel as the principal contaminant. The remaining impurities were almost entirely alkali and alkaline earth metals and their anions which were removed in the plating process. The nickel impurity in the target foils was of no consequence in studying excitation functions of nuclides below  $Z=28$  as the regions around the reaction thresholds were obscured less by contamination from proton reactions on Ni<sup>58</sup> than by neutron background reactions on cobalt and by detection sensitivities. But the excitation function Co<sup>59</sup>( $p,3n$ )Ni<sup>57</sup> was observable to very low cross sections because of the absence of neutron background effects and the lack of interference from other nickel activities. In this case the Ni<sup>58</sup>( $p,pn$ )Ni<sup>57</sup> reaction could interfere seriously. Late in the work a satisfactory method for preparing nickel-free cobalt salts was developed and the nickel-free cobalt target foils obtained were used for studying the Ni<sup>57</sup> reaction.

#### B. Cyclotron Irradiations

The cobalt target foils were bombarded in the energy range up to 100 Mev in the internal scattered beam of the Harvard University 95-in. synchrocyclotron using the well-known stacked-foil technique.<sup>7,8</sup> From four to twenty cobalt foils  $\frac{7}{16}$  in. in diameter and about 50 mg/cm<sup>2</sup> thick were placed in slightly recessed copper foil holders and interspaced with copper absorbers of known thickness to provide simultaneous bombardment of several targets over a considerable energy interval.

<sup>6</sup> O. Sisman and C. D. Bopp, Oak Ridge National Laboratory Report ORNL 299, 1949 (unpublished).

<sup>7</sup> E. O. Lawrence, *Phys. Rev.* **47**, 17 (1935).

<sup>8</sup> N. M. Hintz and N. F. Ramsey, *Phys. Rev.* **88**, 19 (1952).

In this method each of the foils received the same proton flux (with small corrections to be discussed later), and a relative excitation function could be obtained by plotting the yield of a particular activity in each target foil against the proton energy as calculated from the total absorber thickness and the Bethe-Bloch stopping power formula.<sup>9</sup>

The energy resolution of this method was determined chiefly by the diameter of the target foils, and could be approximated at any energy by  $\Delta E \approx \Delta E_0(E_0/E)$ , where  $E_0$  was the initial energy. Two initial energies were available, 73.5 and 100.3 Mev, and for the  $\frac{7}{16}$ -in. diameter foils used,  $\Delta E_0$  was about 0.9 Mev. The proton energy at the front of the stack was determined by running the relative excitation function for the  $C^{12}(p,pn)C^{11}$  reaction in five-minute bombardments on 0.003-in. polyethylene foils and comparing the curves obtained with those of Aamodt, Peterson, and Phillips.<sup>10</sup> The error in the location of the steeply rising portion of the curve in mg/cm<sup>2</sup> copper equivalent was subtracted from the assumed range of the protons at the front of the stack, as the energy error in mg/cm<sup>2</sup> was constant throughout the target. The average correction required was about 200 mg/cm<sup>2</sup> Cu corresponding to a 3-Mev error at 20 Mev. Energy checks were made before every low-energy run. Corrected energies at the front of the target stack were accurate to  $\pm 50$  mg/cm<sup>2</sup> Cu.

The proton flux was monitored by the  $Al^{27}(p,3pn)Na^{24}$  reaction whose excitation function is flat from 70 to 80 Mev.<sup>8</sup> In each run two to four 20-mg/cm<sup>2</sup> aluminum foils were placed in the recessed foil holders along with the cobalt targets, and the 15-hour  $Na^{24}$  activity was measured one day after bombardment. The peak cross section for the aluminum monitor reaction is based on the peak cross section for the  $C^{12}(p,pn)C^{11}$  reaction. This carbon excitation function has recently been remeasured at Berkeley<sup>11</sup> and a new value of 87.5 mb obtained for the peak cross section. All absolute yields reported in this paper are thus based on a corrected  $Al^{27}(p,3pn)Na^{24}$  peak cross section of 14.0 mb.

### C. Linear Accelerator Irradiations

As the energy spread of the cyclotron beam became quite large at low energies, two bombardments were made with the 32-Mev proton linear accelerator at Berkeley to get good resolution in the low-energy portions of the  $Ni^{57}$  and  $Co^{58}$  excitation functions. The target stack consisted entirely of very thin (8–10 mg/cm<sup>2</sup>) cobalt foils covered with a thin cobalt window and imbedded in a brass block. The linear accelerator beam was collimated so that all the incident protons

stopped within the area of the target foils. The energy of the incident protons was known to  $\pm 0.2$  Mev.

### D. Chemistry

After bombardment the cobalt targets were dissolved in hot nitric acid containing 10-mg amounts of carriers for the elements vanadium through nickel. Group separations were used to isolate each of the six elements essentially free from the rest, followed by specific procedures for each element to guarantee purity in the final counting samples. Solvent extraction techniques were used extensively as they were rapid and gave good decontamination factors by avoiding the coprecipitation difficulties inherent in conventional separation schemes. The complete separation scheme is outlined below; in general, at least four elemental fractions were isolated in each bombardment and the exact combination of procedures used varied in each case with the activities to be isolated.

#### Group Separations

After treatment with HCl and  $NaHSO_3$  to reduce higher oxidation states of manganese, chromium, and vanadium, the target solution was diluted to 20 ml and 1M HCl. Vanadium and iron were extracted with successive portions of 10 ml 1% aqueous cupferron and 10 ml chloroform until the extracts were colorless. After washing the combined chloroform phases with 1M HCl, iron was back-extracted with 9M HCl and the back extracts were washed with chloroform.

The aqueous phase from the cupferron extraction was washed with chloroform, 5 ml 6M KOAc added, and cobalt and nickel extracted with 20 ml 10% 8-hydroxyquinoline (oxine) in chloroform. The chloroform extract was washed with HOAc/KOAc buffer at pH 5. The aqueous phase containing chromium and manganese was extracted again with oxine solution, the organic layer discarded, and the aqueous phase washed with chloroform. The nickel-cobalt organic phase and the manganese-chromium aqueous phase were each evaporated over concentrated  $HNO_3$  to the destruction of ammonium salts, and the residues dissolved in concentrated  $HNO_3$ .

The nickel-cobalt fraction was diluted to 1M  $HNO_3$ , an equal volume of 10M NaSCN added and cobalt extracted into 20 ml methyl isobutyl ketone. The organic phase was washed with 5M NaSCN and the aqueous nickel phase washed with methyl isobutyl ketone.

The aqueous phase from the oxine extraction was boiled with 20 ml concentrated  $HNO_3$  and solid  $KClO_3$  added to oxidize manganese to  $MnO_2$ , which was centrifuged off, leaving hexavalent chromium in solution.

#### Purifications

The chloroform solution of vanadium cupferrate was evaporated over concentrated  $HNO_3$ , neutralized with

<sup>9</sup> H. A. Bethe and J. Ashkin in *Experimental Nuclear Physics*, edited by E. Segrè (John Wiley and Sons, Inc., New York, 1953), Vol. I, Part II.

<sup>10</sup> Aamodt, Peterson, and Phillips, *Phys. Rev.* **88**, 739 (1952).

<sup>11</sup> Crandall, Millburn, Pyle, and Birnbaum, *Phys. Rev.* **101**, 329 (1956).

KOAc,  $Pb(NO_3)_2$  added to precipitate  $Pb(VO_3)_2$ , and the precipitate dissolved in 6M  $HNO_3$ . Iron was extracted from the 9M HCl solution with isopropyl ether and back-extracted with water. Cobalt was back-extracted from the methyl isobutyl ketone phase with 3M NaOH, the solution adjusted to pH 5 with HCl and KOAc, potassium cobaltinitrite precipitated, and the precipitate dissolved in HCl. Nickel was precipitated from the aqueous NaSCN solution with NaOH, the solution adjusted to pH 5 with HCl and KOAc, nickel precipitated with dimethylglyoxime, and the precipitate dissolved in  $HNO_3$ . The  $MnO_2$  precipitate was dissolved with  $HNO_3$  and  $H_2O_2$ , evaporated with concentrated  $HNO_3$ ,  $MnO_2$  precipitated on addition of  $KClO_3$ , and the precipitate dissolved with  $H_2O_2$ . The  $HNO_3$  solution of chromium was neutralized with a slight excess of NaOH, the solution chilled,  $H_2O_2$  and  $HNO_3$  added and the chromium extracted into ethyl ether as blue perchromic acid. The chromium was recovered by evaporating the ether phase over 6M HCl.

Two purification cycles were performed on each sample. Tracer studies of the complete separation scheme showed that decontamination factors for the six elemental fractions were at least  $10^6$  with respect to each of the other five carriers originally added.

#### *Preparation of Counting Samples*

With the exception of some of the cobalt and nickel samples, all of the counting was done with a well-type scintillation crystal. The purified counting samples were made up to about five ml, of which 4.00 ml were pipetted into a soft glass vial for insertion in the counting crystal. Chemical yields were determined on a 0.500-ml aliquot of the remaining material.

The cobalt and nickel samples for the Geiger and flow counters were prepared by electroplating onto 1/64 in. thick copper disks. The cobalt samples were plated from a 2M  $NH_4OH$  solution at a current density of 150 ma/cm<sup>2</sup>. The nickel samples were plated from a pH 6 HOAc/ $NH_4OAc$  buffer at a current density of 50 ma/cm<sup>2</sup>. Chemical yields for these samples were obtained directly from the weight of the deposits.

#### *Analyses*

Yield determinations for the scintillator samples were made on aliquots containing 0.5–1.0 mg metal. All the analyses were done colorimetrically; nickel as the dimethylglyoximate in ammoniacal solution after oxidation with bromine, cobalt as the blue thiocyanate complex in an acetone-water mixture, iron as  $FeCl_3$  in 5M HCl, manganese as permanganate after oxidation with  $KIO_4$  in an  $HNO_3/H_3PO_4$  medium, chromium as chromate in NaOH solution, and vanadium as the red-brown peroxide complex in 3M  $HNO_3$ .

#### **E. Counting**

Three counters were used in this work; an argon-filled, chlorine-quenched 3.5-mg/cm<sup>2</sup> mica end-window

Geiger counter (Amperex Corporation, Brooklyn, New York Type 100-CB); a small windowless flow counter operating in the proportional region and using a 95% argon-5%  $CO_2$  mixture; and a well-type sodium iodide (TI) crystal (Harshaw Chemical Company, Type 22) scintillation counter.

The Geiger counter was used for standardization measurements on the other counters and for measuring activities which, because of the similarity of their half-lives, could only be resolved by aluminum absorption curves. All samples counted in the Geiger counter were evaporated or plated onto one-inch diameter copper disks 1/64 in. thick which rested on a 3/64-in. copper block in an aluminum sample card. The active areas of the samples were the same as those of the aluminum monitor foils.

The scintillation and flow counters were standardized for absolute yield calculations by comparing equal aliquots of each activity studied between the scintillation or flow counter and the Geiger counter. Carrier-free preparations ( $<1\mu$  solids) were used for the comparisons to minimize counting corrections. For electron capture activities possessing gamma but no particulate radiation, direct comparison between the scintillation and Geiger counters was impractical due to the strong and inaccurately known dependence of Geiger tube counting efficiency on gamma energy in the kilovolt region. The standardization was made by selecting a number of negatron-emitting nuclides with known decay schemes which emitted a single gamma ray and comparing their counting rates between the scintillation and Geiger counters. Values for the electron capture activities were interpolated from these values.

The flow counter was standardized for the weakly penetrating radiations of the all-electron capture 270-day  $Co^{57}$  by counting equal aliquots of carrier-free  $Ni^{57}$  with the Geiger counter, and, after decay, the  $Co^{57}$  daughter with the flow counter.

The nuclides studied were identified by their chemical behavior in the separation scheme, their half-lives, their beta particle energies using aluminum absorption curves, and by the energies of their gamma rays from integral pulse height measurements with the scintillation counter.

### **III. RESULTS**

#### **A. Calculations**

The raw counting data were corrected for background and coincidence loss (Geiger counter only), and the decay curves resolved into components which were extrapolated back to the end of the bombardment. Further corrections were applied for sample absorption and scattering (Geiger and flow counters only, determined experimentally for each activity), attenuation of the proton beam in the target stack, chemical yield, variations in target foil thickness and for saturation effects when the bombardment time was an appreciable

fraction of the half-lives involved. The data from several bombardments could then be combined to give complete relative excitation functions by plotting the ratio  $A_x/A_m (=S_x)$  versus energy, where  $A_x$  and  $A_m$  were the corrected values for the product activities and aluminum monitor activities respectively.

The absolute yields of the excitation functions  $\sigma_x$  corresponding to the maxima in the relative excitation function curves were calculated from  $S_x^{\max}$  as

$$\sigma_x = S_x^{\max} \left[ \frac{F_a F_n}{F_b F_c} \right]_x \left[ \frac{F_b F_c}{F_a F_n} \right]_m MR \sigma_m,$$

where  $x$  referred to the activity studied and  $m$  to the  $\text{Al}^{27}(p,3pn)\text{Na}^{24}$  monitor reaction. The factor  $F_a$  corrected for absorption of the radiation by the counter window, by the air between the sample and window, and by any aluminum absorber used;  $F_b$  corrected for backscattering from the sample mount. Thick copper mounts were used, and since the saturation backscattering values are insensitive to the counting arrangement within wide limits,<sup>12</sup> published corrections were used.<sup>13</sup> Recent work by Seliger<sup>14</sup> showed that for small-geometry Geiger counting arrangements,  $F_b$  for electrons was 8% greater than for positrons, the effect being independent of atomic number of the backing and energy. This difference was not included in Hintz and Ramsey's<sup>8</sup> work, resulting in an error of +8% in their value of 16.0 mb for  $\sigma_m$  as they standardized the negatron-emitting  $\text{Na}^{24}$  against the  $\text{C}^{11}$  positron activity. This error cancelled out in calculating absolute cross sections of positron activities from the  $\text{Na}^{24}$  monitor; in the case of negatron-emitting nuclides, calculated yields were multiplied by 0.92 to correct for this effect.

$F_c$  corrected for the counting efficiency of the nuclide in the Geiger counter as  $F_c = b/(1-g)$  where  $g$  was the fraction of the activity at zero total absorber due to the hard gamma component of the activity and  $b$  was the fraction of total decays occurring by beta emission. Values for  $b$  were obtained from literature values when available and calculated from beta-decay systematics<sup>15</sup> for those cases where no data existed.

The factor  $F_n$  corrected for neutron background. In general the relative excitation functions did not exhibit a drop to zero observed yield below the extrapolated reaction threshold, but showed a small yield approximately independent of energy down to beyond the proton range in the target stack. This background yield ( $\leq 5\%$  of maximum) was attributed to neutron background in the cyclotron and particularly to secondary neutrons produced in the target stack. Evidence supporting this explanation was found in the nickel

excitation functions; the nuclides observed could not be produced by neutrons on cobalt, and no background yields below threshold were observed.

The factor  $M$  was the mole ratio of aluminum in the standard monitor foil to cobalt in the standard target foil. The factor  $R$  was used when absolute yields were calculated from  $A_x$  values for samples measured in the scintillation and proportional counters and was measured for each activity as described in the foregoing. The factor  $\sigma_m$  was the assumed maximum absolute cross section for the  $\text{Al}^{27}(p,3pn)\text{Na}^{24}$  monitor reaction. The geometry of the Geiger counting arrangement was assumed independent of radiation characteristics for the nuclides studied. Scattering effects caused by the counter housing, sample shelves, and by air between the counter and sample were also assumed invariant for the nuclides studied.<sup>16</sup>

## B. Errors

Estimated total errors were calculated as the square root of the sum of the squares of the individual errors. The errors in the various factors were largely independent of the nuclides studied except for  $e_1$ , the estimated error in the graphical solution for the activity present at the end of bombardment, and  $e_2$ , the error in the counting efficiency  $F_c$ . While  $e_1$  could be estimated quite well,  $e_2$  had to be derived from critical estimates of literature claims for positron to electron capture ratios. At present the values for the branching ratios constitute the weakest link in the calculations of the absolute cross sections with values of  $e_2$  as high as  $\pm 30\%$ . The other large uncertainty arose from the uncertainty in  $\sigma_m$ , taken as  $\pm 15\%$ .

The error in the absolute cross sections at maximum was  $e_x = \pm (e_1^2 + e_2^2 + 239)^{1/2}\%$ . At low values on the relative excitation functions, errors increased due to the weaker activities present and the increased difficulties in resolving the decay curves. The error over a complete relative excitation function is then probably best represented as  $e_r = \pm (e_1^2 + 6)^{1/2}$  units on the relative cross-section scale.

## C. Data

After computing the values of the ratio  $S_x$  and plotting the curves obtained, the results were normalized to 100 on the relative cross-section scale. Because of interference by other isotopic activities or by neutron background effects, the sensitivity of the experiments did not in general exceed one relative cross-section unit; for this reason logarithmic plots of the excitation functions did not seem justified. But the data for the  $\text{Co}^{59}(p,3n)\text{Ni}^{57}$  was plotted semilogarithmically as this was the only case where the above interferences were absent and where observed activities were intense enough to allow measurement of yields less than 1% of maximum.

<sup>16</sup> L. T. Zumwalt, Oak Ridge National Laboratory Report AECU-567, March, 1950 (unpublished).

<sup>12</sup> B. P. Burt, *Nucleonics* 5, 28 (1949).

<sup>13</sup> L. Yaffe and K. M. Justus, *J. Chem. Soc., Suppl.* 72, S 341 (1949).

<sup>14</sup> H. H. Seliger, *Phys. Rev.* 78, 491 (1950); 88, 408 (1952).

<sup>15</sup> E. Feenberg and G. Trigg, *Revs. Modern Phys.* 22, 402 (1950).

With the exception of the nickel nuclides and the shielded nuclides  $\text{Co}^{58}$  and  $\text{Mn}^{54}$ , the general problem arose of deducing independent yields from observed yields. The nuclides  $\text{Co}^{56}$ ,  $\text{Co}^{57}$ ,  $\text{Mn}^{52}$ , and  $\text{V}^{48}$  had unstable parents whose yields were measured allowing corrections for the contribution of parent decay to the daughter yield. The remaining products had parents which were very short lived or unknown. In these cases, reported yields were those of the isobaric chains starting with the product and extending away from the line of maximum stability to a limit of  $Z=28$  or  $N=32$ . As this study and others<sup>1,17</sup> have shown, yields in any isobaric chain decrease by factors 10-100 per unit change in  $Z$  for products two or more removed from the line of maximum stability, and thus nearly all the observed yield for products with very short-lived parents was independent yield.

The relative excitation functions for the 18 nuclear reactions studied are given in Figs. 1-8. Table I gives the absolute cross sections at maximum ( $\sigma_x$ ) together with the errors  $e_1$ ,  $e_2$ , and  $e_x$ . The branching ratios used (b) are also included.

*Nickel-56.*—Due to the very low yield of this reaction coupled with its unfavorable counting characteristics, no 6.4-day activity was observed in samples counted with the Geiger counter. When the scintillation counter became available,  $\text{Ni}^{56}$  was observed although the  $\text{Ni}^{57}$  product, formed in much higher yield, obscured the  $\text{Ni}^{56}$  until about 14 days after bombardment. By this time only about  $\frac{1}{4}$  of the  $\text{Ni}^{56}$  remained and this was

TABLE I. Maximum cross sections for 0- to 100-Mev protons on cobalt.

Fig.	Reaction	b	$e_1$	$e_2$	$\sigma_x$ (mb) <sup>a</sup>	$e_x$ (mb)
3	$\text{Co}^{59}(p,4n)\text{Ni}^{56}$	25 <sup>b</sup>	3%	20%	0.47	$\pm 0.12$
2	$\text{Co}^{59}(p,3n)\text{Ni}^{57}$	50	1	25	16.1	4.7
4	$\text{Co}^{59}(p,p4n)\text{Co}^{56}$	60	2	25	11.8	3.5
3	$\text{Co}^{59}(p,p3n)\text{Co}^{56}$	25	3	20	8.5	29
2	$\text{Co}^{59}(p,p2n)\text{Co}^{57}$	50 <sup>c</sup>	5	25	157	47
1	$\text{Co}^{59}(p,pn)\text{Co}^{58m}$	15 <sup>d</sup>	1	25	403	120
1	$\text{Co}^{59}(p,pn)\text{Co}^{58+58m}$	15	4	25	675	202
6	$\text{Co}^{59}(p,2p6n)\text{Fe}^{52}$	40	2	30	0.44	0.15
5	$\text{Co}^{59}(p,2p5n)\text{Fe}^{53}$	100	5	20	6.2	1.5
7	$\text{Co}^{59}(p,3p6n)\text{Mn}^{51}$	100	5	20	4.2	1.1
6	$\text{Co}^{59}(p,3p6n)\text{Mn}^{52m}$	100	7	2	11.4	1.9
6	$\text{Co}^{59}(p,3p5n)\text{Mn}^{52}$	35	1	25	17.6	5.7
4	$\text{Co}^{59}(p,3p3n)\text{Mn}^{54}$	0 <sup>e</sup>	1	1 <sup>h</sup>	67	16 <sup>j</sup>
3	$\text{Co}^{59}(p,3pn)\text{Mn}^{56}$	100	2	1	11.5	1.8
8	$\text{Co}^{59}(p,4p8n)\text{Cr}^{48}$	58 <sup>f</sup>	3	15	0.089	0.018
7	$\text{Co}^{59}(p,4p5n)\text{Cr}^{51}$	0 <sup>g</sup>	2	20 <sup>i</sup>	40	13 <sup>k</sup>
8	$\text{Co}^{59}(p,5p7n)\text{V}^{48}$	58	1	15	6.4	1.4
5	$\text{Co}^{59}(p,5p2n)\text{V}^{53}$	100	5	20	0.04	0.01

<sup>a</sup> Based on value of maximum cross section for  $\text{Al}^{27}(p,3pn)\text{Na}^{24}$  of 14.0 mb which, in turn, is based on value of peak cross section for  $\text{C}^{12}(p,pn)\text{C}^{11}$  of 87.5 mb (see reference 11).

<sup>b</sup>  $\text{Co}^{56}$  daughter.

<sup>c</sup>  $\text{Ni}^{57}$  parent.

<sup>d</sup>  $\text{Co}^{58}$  daughter.

<sup>e</sup> 100% decay through 0.84 Mev gamma assumed.

<sup>f</sup>  $\text{V}^{48}$  daughter.

<sup>g</sup> 8% decay through 0.33-Mev gamma assumed.

<sup>h</sup> Estimated error in abundance of 0.84-Mev gamma.

<sup>i</sup> Estimated error in abundance of 0.33-Mev gamma.

<sup>j</sup> Error in R estimated as 20%.

<sup>k</sup> Cross section at 100 Mev.

<sup>17</sup> Rudstam, Stevenson, and Folger, Phys. Rev. 87, 358 (1952).

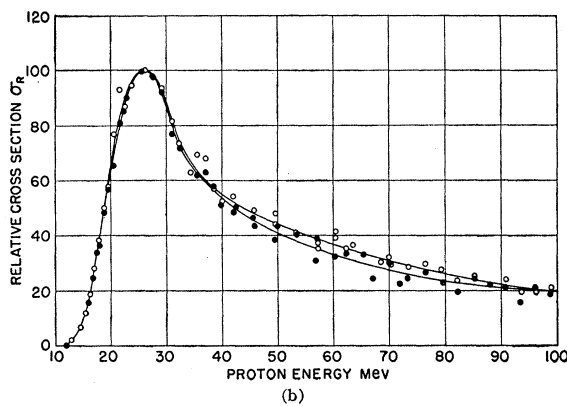
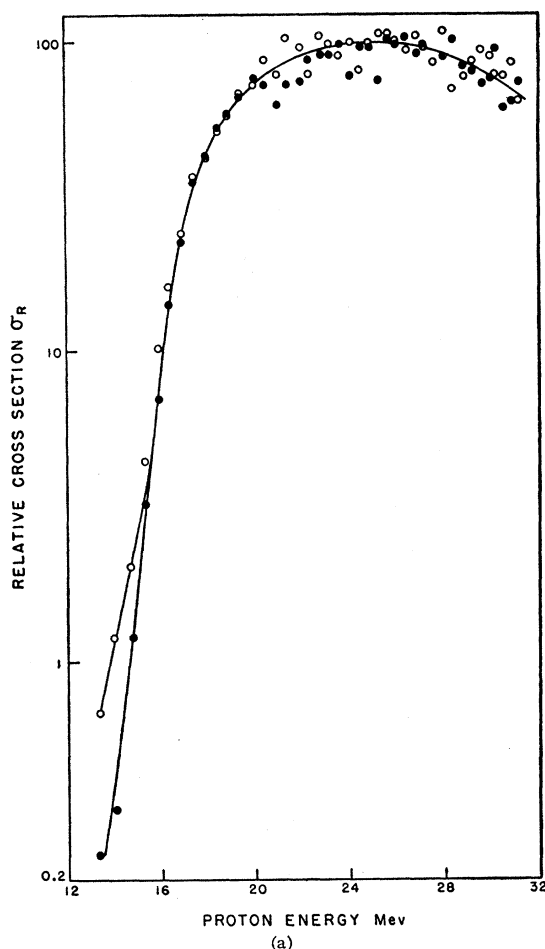


FIG. 1. (a)  $\text{Co}^{59}(p,pn)\text{Co}^{58,58m}$  linear accelerator data;  $\bullet$   $\text{Co}^{58}$ ,  $\circ$   $\text{Co}^{58m}$ . (b)  $\text{Co}^{59}(p,pn)\text{Co}^{58,58m}$  cyclotron data;  $\bullet$   $\text{Co}^{58}$ ,  $\circ$   $\text{Co}^{58m}$ .

soon obscured by the  $\text{Co}^{56}$  daughter which counted much more efficiently. In order to see an unambiguous 6.4-day decay, it was necessary to milk the nickel fraction free of cobalt about two weeks after bombardment before counting the  $\text{Ni}^{56}$ . Even with an eight-hour bombardment the hottest samples showed activities only about twice background.

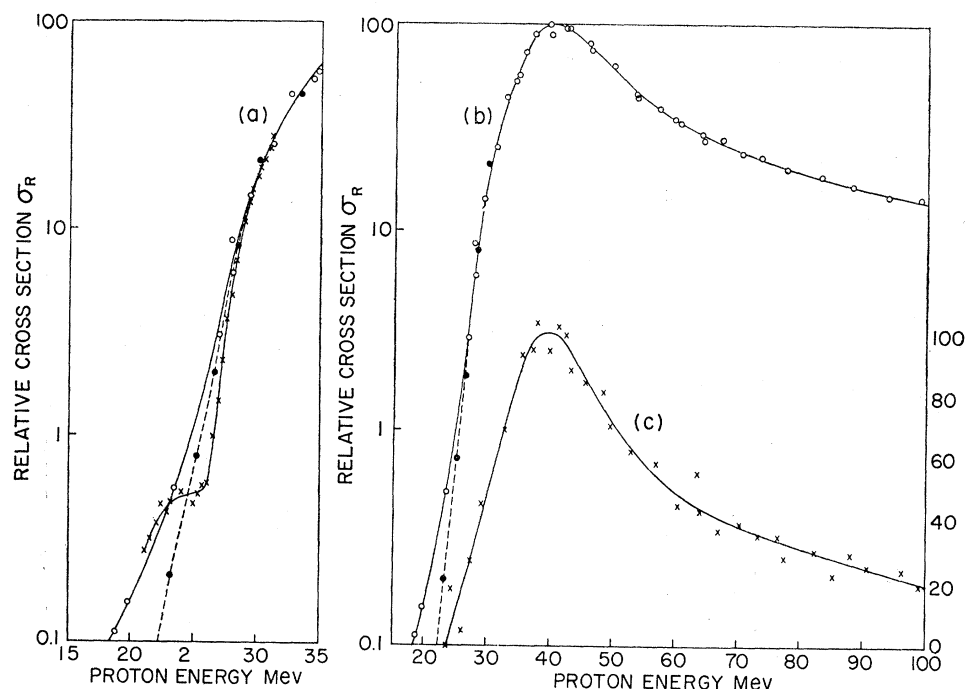


FIG. 2.  $\text{Co}^{58}(p,3n)\text{Ni}^{57}$  curves (a): cyclotron data,  $\circ$  0.1% Ni in target;  $\bullet$   $<10^{-4}\%$  Ni in target; linear accelerator data  $\times$ .  $\text{Co}^{58}(p,3n)\text{Ni}^{57}$  curves (b): cyclotron data,  $\circ$  0.1% Ni in target;  $\bullet$   $<10^{-4}\%$  Ni.  $\text{Co}^{58}(p,p2n)\text{Co}^{57}$ , curves (c)  $\times$ .

*Nickel-57.*—Most of the data for this reaction were obtained with a Geiger counter. When the scintillator became available, the data were extended to low-yield values near threshold. Later in the work a low-energy linear-accelerator bombardment was made primarily to obtain data on the  $\text{Co}^{58}/\text{Co}^{58m}$  isomeric pair. Nickel samples were also isolated from this run and the data were combined with that from the cyclotron runs. As expected, the linac data fell off more sharply near threshold, reflecting the narrower energy distribution of the protons from that machine. The break in the linac data near 25 Mev was attributed to interference from the  $\text{Ni}^{58}(p,pn)\text{Ni}^{57}$  on the nickel impurity in the target foil. A cyclotron run with a specially purified target very low in nickel showed lowered yields near

threshold, consistent with the foregoing explanation (Fig. 2).

*Cobalt-56.*—Because of simultaneous production of  $\text{Co}^{58}$  with the same 72-day half-life, it was necessary to take aluminum absorption curves on each sample to separate the two activities. The low cross section of  $\text{Co}^{56}$  relative to  $\text{Co}^{58}$  increased the difficulty of resolution, but this was largely compensated for since the much harder  $\text{Co}^{56}$  beta particles could be measured through thick absorbers with little interference from the softer  $\text{Co}^{58}$  radiation.

*Cobalt-57.*—The long (270-day) half-life of this isotope made it inconvenient to separate it from the 72-day  $\text{Co}^{56}$  and  $\text{Co}^{58}$  activities by decay-curve analysis. The decay scheme of  $\text{Co}^{57}$  ( $>99\%$  electron capture) increased the difficulties of measurement.  $\text{Co}^{57}$  was first observed through integral pulse height curves taken with the scintillation counter which showed a soft gamma component in the cobalt samples (the 119- and 131-keV  $\text{Co}^{57}$  gammas). Quantitative measurement of the  $\text{Co}^{57}$  in the presence of the much larger Compton continuum from the other cobalt activities was not practical. Because of the elimination of air and window absorption of the iron x-rays emitted by  $\text{Co}^{57}$ , the windowless flow counter showed much greater sensitivity in this case and also had several-fold better geometry. Standards of various weights containing known amounts of  $\text{Co}^{56}$  and  $\text{Co}^{58}$  were compared between the Geiger and flow counters, so that the net activity expected in the flow counter from these activities alone could be calculated from the results of the aluminum absorption measurements on the cobalt samples. The excess

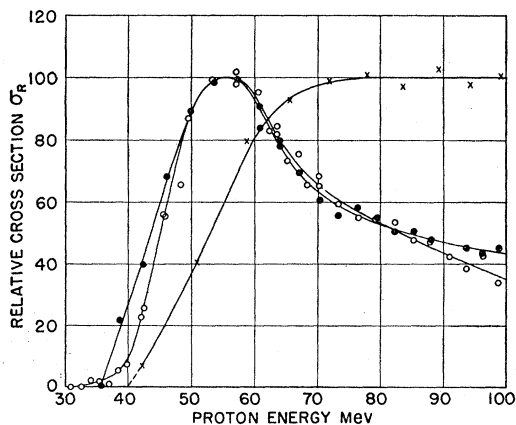


FIG. 3.  $\text{Co}^{59}(p,4n)\text{Ni}^{56}$   $\bullet$ ;  $\text{Co}^{59}(p,3pn)\text{Mn}^{56}$   $\times$ ;  $\text{Co}^{59}(p,3n)\text{Co}^{56}$   $\circ$ .

activity observed in the flow counter was then attributed to  $\text{Co}^{57}$ .

*Iron-53, Manganese-51, Manganese-52m, and Manganese-56.*—These short-lived activities (9 min, 44 min, 21 min, and 2.6 hr, respectively) were measured by direct counting of the cobalt target foils after 10-minute bombardments. The samples were counted through  $268 \text{ mg/cm}^2$  of aluminum which suppressed considerably the longer lived activities formed while passing most of the radiations of these short-lived high-energy beta emitters. The activities were separated by decay-curve analysis. High levels of activity were available which gave good statistics with the necessarily short counting times used. About eight minutes elapsed between the end of the bombardment and the first points on the decay curves. While the 9-min  $\text{Fe}^{53}$  and 2.6-hr  $\text{Mn}^{56}$  activities stood out well against the background, some difficulty was experienced in resolving the 44-min  $\text{Mn}^{51}$  and 21-min  $\text{Mn}^{52m}$  activities, resulting in lowered accuracy for these excitation functions.

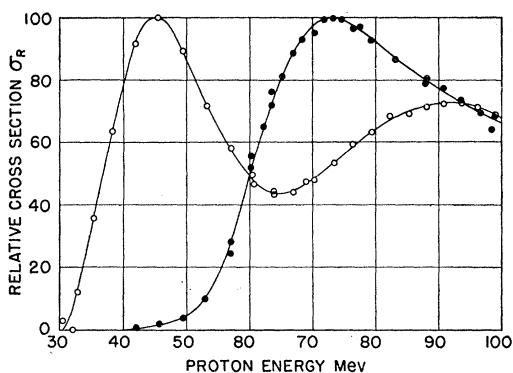


FIG. 4.  $\text{Co}^{59}(p,p4n)\text{Co}^{56}$  ●;  $\text{Co}^{59}(p,3p3n)\text{Mn}^{54}$  ○.

*Manganese-54.*—This activity was measured in the scintillation counter by counting the 0.84-Mev gamma accompanying its electron capture decay. The double maximum shown by this excitation function (Fig. 4) was in contrast to the behavior of the other curves. Repurification of the manganese samples produced no change in the data and samples followed for over a year showed 300 days at both maxima. Integral pulse-height curves on the samples showed the complete curve to be composed of a single gamma activity of 800- to 900-kev energy. As  $\text{Mn}^{53}$  is still uncharacterized, the remote possibility exists that it also has an approximately 300-day half-life with nearly the same radiations. But the wide separation of the peaks precludes the possibility that the curve is the result of two superimposed excitation functions for products only one mass number apart.

*Chromium-48.*—As the decay scheme for this isotope was not known, and as it was reported to decay entirely by electron capture,<sup>17</sup> no attempt was made to measure its yield directly. Instead purified chromium fractions

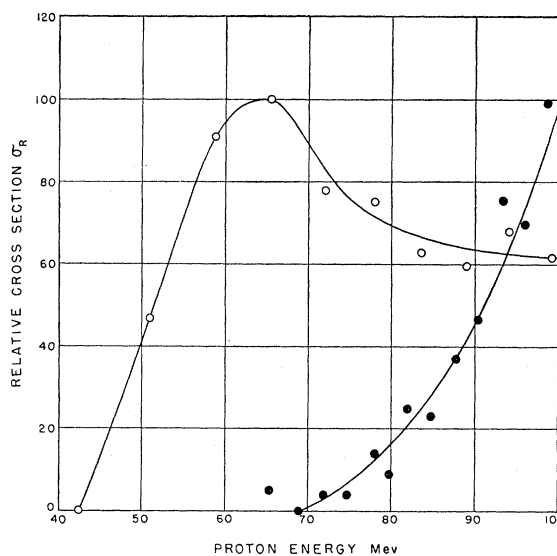


FIG. 5.  $\text{Co}^{59}(p,2p5n)\text{Fe}^{53}$  ○;  $\text{Co}^{59}(p,5p2n)\text{V}^{53}$  ●.

prepared shortly after bombardment were allowed to decay for about two weeks, after which vanadium carrier was added and the  $\text{V}^{48}$  daughter activity recovered.

*Limitations.*—The available proton flux in the cyclotron coupled with the counting efficiencies of the detectors prevented the measurement of certain long-lived activities in this region. Thus while 270-day  $\text{Co}^{57}$  was observed because of its high yield and 310-day  $\text{Mn}^{54}$  because of its high counting efficiency, attempts to measure 635-day  $\text{V}^{49}$  gave negative results. The maximum yield of  $\text{V}^{49}$  certainly occurs below 100 Mev and is of the order of 40 mb, but in the absence of beta or

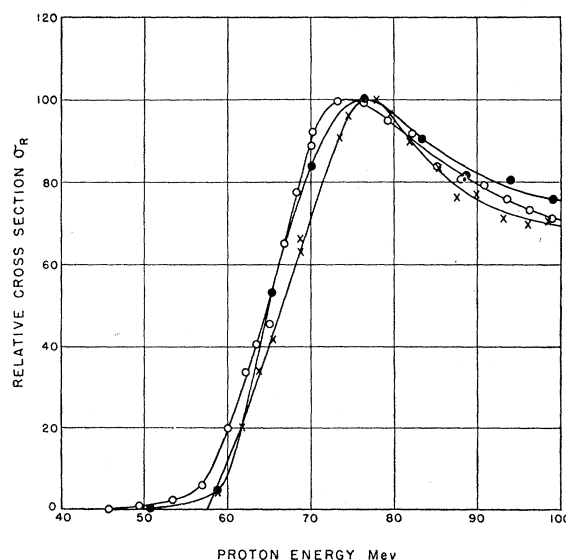


FIG. 6.  $\text{Co}^{59}(p,2p6n)\text{Fe}^{52}$  x;  $\text{Co}^{59}(p,3p5n)\text{Mn}^{52}$  ○;  $\text{Co}^{59}(p,3p5n)\text{Mn}^{52m}$  ●.

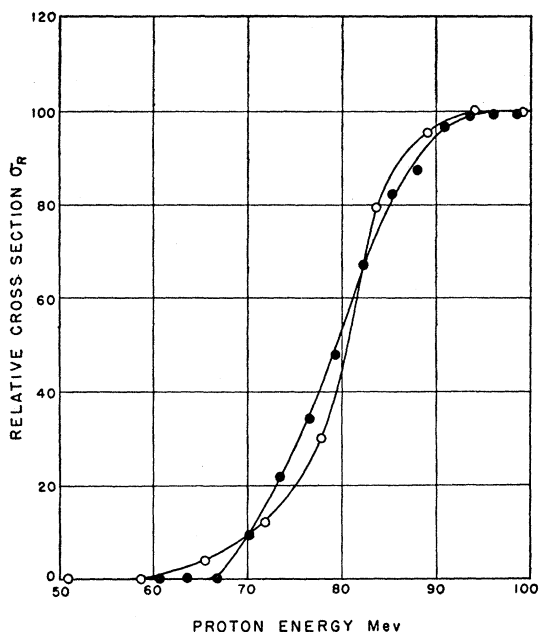


FIG. 7.  $\text{Co}^{59}(p,3p6n)\text{Mn}^{51}$  ○ ;  $\text{Co}^{59}(p,4p5n)\text{Cr}^{51}$  ●.

hard gamma radiation it is not surprising that it escaped detection.

Attempts to measure an excitation function for 2.9-year  $\text{Fe}^{55}$  proved unsatisfactory. Old iron-fraction samples in the form of  $\text{Fe}_2\text{O}_3$  showed activities up to five times background in the flow counter. The very high chemical purity of these samples plus the absence of beta radiation was good assurance that the activity observed was due to  $\text{Fe}^{55}$ . The large scatter in the data was doubtless due to difficulties in preparing evenly distributed samples, as small variations in sample thickness have a large effect on specific activity for radiations below 10 kev. The data indicated a threshold for the  $\text{Co}^{59}(p,2p3n)\text{Fe}^{55}$  reaction at about 15–20 Mev with a definite peak at 65–70 Mev and a possible second peak at 22–27 Mev. The yield at maximum was estimated at about 220 mb.

#### IV. DISCUSSION

##### A. Interaction Models

Nuclear reactions of protons with cobalt in the energy range up to 100 Mev are of the type  $A + p = X + x + \gamma$ , where  $A$  is the cobalt target,  $p$  the proton projectile,  $X$  the heavy fragment produced (mass  $\sim 40$ – $60$ ),  $x$  the collection of light fragments produced (almost entirely of mass  $\leq 4$ ) and  $\gamma$  the electromagnetic radiation accompanying the reaction. Fissioning of the cobalt target nucleus into two or more fragments of roughly equal mass is also possible at these energies but the cross sections for these processes are very low ( $\leq 0.01$  mb for  $\text{Cl}^{34+38}$ ).<sup>3</sup>

Several types of experiments have been used to study nuclear reactions, including cloud-chamber studies,

scattering measurements, emulsion experiments, and radiochemical yield studies. Information available includes the angular distribution and energy spectrum of the emitted fragments, the multiplicity of products formed, the total cross section of the interaction, the charge and mass distribution of the products, and the yields of individual nuclear species. The areas covered by the separate experiments overlap considerably. This study produced no information in the first two categories and was most useful for the results obtained in the last two.

The conceptual framework for the understanding of nuclear reactions in the low-energy region was laid by Bohr<sup>18</sup> in his formulation of the compound nucleus theory. Bohr pictured nuclear reactions as occurring in two stages. First the projectile enters the nucleus bringing in its kinetic plus binding energy. Since the life of the compound nucleus formed is long ( $\sim 10^{-14}$  sec) as compared to the transit time of a nucleon across the nucleus ( $\sim 10^{-21}$  sec), there is a statistical sharing of the energy brought in among all the nucleons. In the second stage, statistical fluctuations cause enough energy to become locally concentrated to allow de-excitation of the compound nucleus by particle emission and by radiation. Because of the long life of the compound nucleus, an essential result of this theory is that the evaporation step should not depend on how the compound nucleus was formed. Ghoshal<sup>19</sup> demonstrated the equivalence of the  $\text{Zn}^{64}$  compound nuclei formed in proton bombardment of  $\text{Cu}^{63}$  and alpha bombardment of  $\text{Ni}^{60}$  by obtaining equivalent excitation functions for

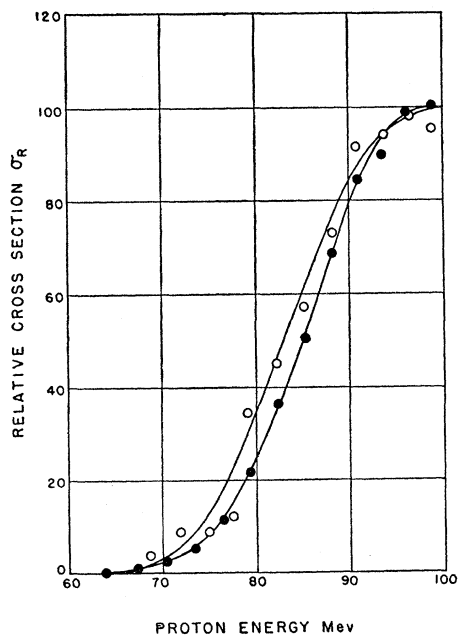


FIG. 8.  $\text{Co}^{59}(p,4p8n)\text{Cr}^{48}$  ○ ;  $\text{Co}^{59}(p,5p7n)\text{V}^{48}$  ●.

<sup>18</sup> N. Bohr, Nature 137, 344 (1936).

<sup>19</sup> S. N. Ghoshal, Phys. Rev. 80, 939 (1950).

the Zn<sup>62</sup>, Zn<sup>63</sup>, and Cu<sup>62</sup> products formed in the two bombardments when results were compared at equal excitation energies. The angular distribution of fragments emitted by the compound nucleus should be symmetric about 90° in the center-of-mass system, and might be isotropic; this has been demonstrated for reactions at low energies.<sup>20,21</sup>

As the bombarding energy of the projectile is increased, the Bohr theory predicts a sharp peak in the cross section for the reaction (*p,a*), where a single nucleon is emitted, followed by a rapid decline in yield as the excitation energy becomes sufficient to evaporate a second particle. Similar sharp peaks are expected for the families (*p,abc*), etc., with reactions of lower order having negligible yield well beyond the maxima of those of next higher order. Such peaks have been observed in many low-energy nuclear reactions,<sup>22</sup> but the yields at higher energy do not decrease to very low values as predicted. (See also the excitation functions for Co<sup>58</sup> and for Co<sup>57</sup>, Figs. 1 and 2.) Examination of the series of reactions (*p,pn*), (*p,p2n*), (*p,p3n*) and (*p,p4n*) (Figs. 1-4) shows that agreement with the qualitative predictions of the Bohr model deteriorated as the multiplicity of the reaction and the bombarding energy increased. Also, at bombarding energies  $\geq 100$  Mev the Bohr model predicts a distribution of products with maximum yields concentrated many mass numbers below the target. A wide distribution of yields has been found in high-energy spallation investigations but the maximum yields are always found in the immediate vicinity of the target.<sup>1,23,24</sup>

In view of these difficulties, Serber<sup>25</sup> proposed a new model for the initial high-energy interaction. The validity of the Bohr model decreases at higher energies since the de Broglie wavelength of the incident nucleon becomes of the same order as the nucleon-nucleon distance in the nucleus. The time of collision between the projectile and target nucleons becomes short compared to the time of transit of nucleons across the nucleus, and since the cross section for scattering decreases with energy while the mean free path increases, the phenomenon of partial nuclear transparency sets in. Thus a typical 100-Mev proton incident on a cobalt nucleus experiences only a few collisions with target nucleons and emerges with a large fraction of its initial energy. The struck nucleons, with their much lower kinetic energy and correspondingly shorter mean free path in nuclear matter, may escape from the nucleus as "knock-on" particles if generated near the surface and directed outwards; otherwise there is a large probability for collision with other target nucleons with gradual transfer of energy until thermal capture occurs.

The generation of the Serber internal nucleonic cascade requires of the order of 10<sup>-21</sup> second and culminates with the formation of excited nuclei possessing a wide range of excitations. The excited nuclei then dissipate their energy by evaporating other particles as in the Bohr compound nucleus picture. This model qualitatively explains the wide distribution of spallation products at high energies by allowing for a wide range of excitation energies; the high yields in the vicinity of the target are the result of nuclear transparency where the projectile has only one or two collisions inside the nucleus depositing little excitation energy. At lower energies, this model becomes indistinguishable from the Bohr model, and thus the range of behavior represented in the Co<sup>55-58</sup> excitation functions is understandable.

Goldberger<sup>26</sup> has formulated a detailed model of the knock-on process in high-energy reactions, which is in qualitative agreement with experiment.<sup>27,28</sup> Bernardini, Booth, and Lindenbaum,<sup>29</sup> and Meadows<sup>30</sup> have used a combination knock-on plus subsequent nucleon evaporation model for calculations of high-energy reactions. In spite of the simplifying assumptions made in order to obtain answers without an unreasonable expenditure of time and effort, good agreement with their experimental results was obtained, such agreement substantiating the existence of both types of mechanisms.

## B. Emission of Heavy Charged Particles

The possibility of the emission of charged particles such as deuterons, tritons, alpha particles, and heavier fragments was ignored in the Goldberger-type calculations mentioned above. This could be a serious omission, as such particles are certainly ejected in the energy range up to 100 Mev. Examination of the

TABLE II. Threshold calculations.

Product nuclide	Reaction mechanism	-Q (Mev)	-Q+V <sub>b</sub> (Mev)
Mn <sup>54</sup>	( <i>p,Li<sup>6</sup></i> )	14.3	32
	( <i>p,αd</i> )	15.9	34
	( <i>p,αpn</i> )	18.1	36
	( <i>p,H<sup>3</sup>He<sup>3</sup></i> )	30.2	48
	( <i>p,H<sup>2</sup>p2n</i> )	37.9	59
	( <i>p,He<sup>3</sup>p2n</i> )	38.6	57
	( <i>p,2d<p2n< i=""></p2n<></i> )	41.9	63
	( <i>p,d2p2n</i> )	44.1	65
	( <i>p,3p3n</i> )	46.3	68
	( <i>p,4p5n</i> )	73.8	102
Cr <sup>51</sup>	( <i>p,2αn</i> )	18.0	40
	( <i>p,α2p3n</i> )	45.9	57
V <sup>48</sup>	( <i>p,5p7n</i> )	103.8	139
	( <i>p,2αp3n</i> )	48.0	77
	( <i>p,α3p5n</i> )	75.9	108

<sup>20</sup> G. A. Price, Phys. Rev. **93**, 1279 (1954).

<sup>21</sup> Geller, Halpern, and Yergin, Phys. Rev. **95**, 659 (1954).

<sup>22</sup> J. W. Meadows, Phys. Rev. **91**, 885 (1953).

<sup>23</sup> Batzel, Miller, and Seaborg, Phys. Rev. **84**, 671 (1951).

<sup>24</sup> H. H. Hopkins, Jr., Phys. Rev. **77**, 717 (1950).

<sup>25</sup> R. Serber, Phys. Rev. **72**, 1114 (1947).

<sup>26</sup> M. K. Goldberger, Phys. Rev. **74**, 1269 (1948).

<sup>27</sup> J. A. Hofmann and K. Strauch, Phys. Rev. **90**, 449 (1953).

<sup>28</sup> J. Hadley and H. York, Phys. Rev. **80**, 345 (1950).

<sup>29</sup> Bernardini, Booth, and Lindenbaum, Phys. Rev. **85**, 826 (1952), and Phys. Rev. **88**, 1017 (1952).

<sup>30</sup> J. W. Meadows, Phys. Rev. **91**, 885 (1953); Phys. Rev. **98**, 744 (1955).

TABLE III. Cobalt and copper reaction yields.

Reaction	Odd-even character <i>Z-N</i>	Energy at curve max Mev	$\sigma_{\alpha}^a$ mb	$\sigma_{100 \text{ Mev}}^a$ mb	$(\sigma_{\alpha})_{\text{Co}}$ $(\sigma_{\alpha})_{\text{Cu}}$	$(\sigma_{100 \text{ Mev}})_{\text{Co}}$ $(\sigma_{100 \text{ Mev}})_{\text{Cu}}$
Cu <sup>63</sup> ( <i>p,pn</i> )Cu <sup>62</sup>	<i>O-O</i>	27	500	96	1.35	1.28
Cu <sup>65</sup> ( <i>p,pn</i> )Cu <sup>64</sup>	<i>O-O</i>	25	464	140	1.45	0.96
Co <sup>59</sup> ( <i>p,pn</i> )Co <sup>58</sup>	<i>O-O</i>	26	675	135		
Cu <sup>63</sup> ( <i>p,p2n</i> )Cu <sup>61</sup>	<i>O-E</i>	38	297	61	0.53	0.51
Co <sup>59</sup> ( <i>p,p2n</i> )Co <sup>57</sup>	<i>O-E</i>	39	157	31.5		
Cu <sup>65</sup> ( <i>p,p3n</i> )Cu <sup>62</sup>	<i>O-O</i>	47	175	61	0.49	0.49
Co <sup>59</sup> ( <i>p,p3n</i> )Co <sup>56</sup>	<i>O-O</i>	56	85	29.8		
Cu <sup>65</sup> ( <i>p,p4n</i> )Cu <sup>61</sup>	<i>O-E</i>	62	70	30.6	0.17	0.25
Co <sup>59</sup> ( <i>p,p4n</i> )Co <sup>55</sup>	<i>O-E, N magic</i>	74	11.8	7.8		
Cu <sup>65</sup> ( <i>p,3n</i> )Zn <sup>63</sup>	<i>E-O</i>	37	145	9.6	0.11	0.22
Co <sup>59</sup> ( <i>p,3n</i> )Ni <sup>57</sup>	<i>E-O, Z magic</i>	40	16.1	2.28		
Cu <sup>65</sup> ( <i>p,4n</i> )Zn <sup>62</sup>	<i>E-E</i>	50	17.5	3.5	0.027	0.057
Co <sup>59</sup> ( <i>p,4n</i> )Ni <sup>56</sup>	<i>E-E, N magic</i> <i>Z magic</i>	56	0.47	0.201		

<sup>a</sup> Based on value of maximum cross section for Al<sup>27</sup>(*p,p3n*)Na<sup>24</sup> of 14.0 mb, which in turn is based on value of peak cross section for C<sup>12</sup>(*p,pn*)C<sup>11</sup> of 87.5 mb (see reference 11).

excitation functions in this study shows that many of the thresholds observed cannot possibly be those due to simple-particle emission only. Table II lists  $-Q$  values and  $-Q+V_b$  values (classical threshold assuming no barrier penetration) for a number of possible mechanisms to form the nuclides Mn<sup>54</sup>, Cr<sup>51</sup>, and V<sup>48</sup>.

In the case of Mn<sup>54</sup> all possible mechanisms involving the particles *n*, *p*, *d*, H<sup>3</sup>, He<sup>3</sup>, He<sup>4</sup>, and Li<sup>6</sup> are listed. It is seen that only the first four mechanisms can explain the yield below 38 Mev. Undoubtedly a mixture of mechanisms contributes to the yield over most of the excitation curve, but from the observations of Hadley and York,<sup>28</sup> Waniek and Ohtsuka<sup>31</sup> and Deutsch<sup>32</sup> it can be said that protons, deuterons and alphas are the only charged particles ejected in large yield (>5%) at energies up to 100 Mev. Thus the first maximum in the Mn<sup>54</sup> excitation function represents a large contribution from alpha particle mechanisms, while the second maximum represents yields largely to proton and deuteron emission. Examination of the thresholds and  $-Q$  values for Cr<sup>51</sup> and V<sup>48</sup> gives further evidence for alpha emission. Similar arguments can be made with the remaining neutron-deficient products of iron, manganese, chromium, and vanadium. Other excitation function studies have also shown evidence for alpha-particle emission.<sup>33,34</sup> Evidently such groupings become highly probable when the economies afforded by the high binding energy of the alpha particle becomes important.

### C. Effects of Nuclear Shell Structure

If the excitation functions in this study are compared with those obtained by Meadows<sup>30</sup> for protons on copper, some striking differences are apparent in the magnitudes of the observed yields. Table III gives the

absolute yields at the cross-section maximum and at 100 Mev for similar reactions studied for both targets and includes a notation describing the odd-even character of the product nuclides. In the last two columns the cobalt and copper cross sections are compared. Since cobalt differs only slightly from copper in atomic weight and since the proton-neutron ratios are almost identical (2.19 and 2.21 respectively), similar cross sections might be expected for the same reactions. While the (*p,pn*) cross sections agree within experimental errors, the other reactions show significant deviations with the yields of the magic number products Co<sup>55</sup> (*N*=28), Ni<sup>57</sup> (*Z*=28) and especially the doubly magic Ni<sup>56</sup> (*Z* and *N*=28) being particularly low.

A large amount of evidence exists which shows that certain numbers of neutrons and protons form nuclei with especially stable configurations. Several authors<sup>35-38</sup> have been able to derive the level structure yielding shell closures at the magic numbers of *N* or *Z*=2, 8, 14, 20, 28, 50, 82, and 126. The influence of the shell structure on reaction cross sections is best understood by assuming that magic-number nuclei have abnormally low-level densities. It then follows from the statistical theory of Weisskopf<sup>39-41</sup> that the probability of an evaporation step decaying to a magic number product is depressed. Because of the excitation produced in the knock-on process, evaporation dominates in the last steps of de-excitation, and thus the yield of all magic-number products should be low. A similar effect was seen by Meadows<sup>30</sup> where the yields of odd-odd and even-even nuclei in (*p,pn*) and (*p,2n*) reactions were measured. He found that cross sections for the odd-odd

<sup>28</sup> Hazel, Jensen, and Suess, Phys. Rev. **75**, 1766 (1949).

<sup>29</sup> M. G. Mayer, Phys. Rev. **75**, 1969 (1949); **78**, 16 and 22 (1950).

<sup>30</sup> E. Feenberg and K. C. Hammack, Phys. Rev. **75**, 1877 (1949).

<sup>31</sup> L. W. Nordheim, Phys. Rev. **75**, 1894 (1949).

<sup>32</sup> V. F. Weisskopf, Phys. Rev. **52**, 295 (1937).

<sup>33</sup> V. F. Weisskopf and D. H. Ewing, Phys. Rev. **57**, 472 (1940).

<sup>31</sup> R. W. Waniek and T. Ohtsuka, Phys. Rev. **89**, 1307 (1953).

<sup>32</sup> R. W. Deutsch, Phys. Rev. **90**, 499 (1953); Phys. Rev. **97**, 1110 (1955).

<sup>33</sup> F. O. Bartell and S. Softky, Phys. Rev. **84**, 463 (1951).

<sup>34</sup> J. W. Meadows and R. B. Holt, Phys. Rev. **83**, 47 and 1257 (1951).

<sup>39</sup> J. Blatt and V. F. Weisskopf, *Theoretical Nuclear Physics* (John Wiley and Sons, Inc., New York, 1952).

products were favored and that his results were consistent with statistical theory only if he assumed that the level densities of odd-odd nuclei were four to ten times as great as for even-even nuclei.

The cobalt and nickel yields reported here are presumably also depressed by the odd-even effect, but since copper and zinc products with the same odd-even properties were chosen for comparison, the discrepancies observed should be largely due to shell closure effects. The low-level densities observed for magic-number nuclei in thermal-neutron capture reactions appear to approach normal values at higher excitation energies.<sup>42</sup> The level densities of even-even and odd-odd nuclei may also well behave similarly. Such would be the case if the energy-level density had the dependence suggested by Hurwitz and Bethe,<sup>43</sup> that is, that the excitation energy,  $E$ , used in the formula  $\omega(E) = C \exp[2(aE)^{1/2}]$ , be measured, not from the ground state but from a characteristic level that varies smoothly from nucleus to nucleus. The actual ground states of magic number and of even-even nuclei would be depressed below this characteristic level compared to those of odd mass and especially of odd-odd nuclei, and so, at low excitation (above the ground state) the former nuclei would have very small level densities compared to the latter. As the excitation energy is raised the relatively small energy differences between ground and characteristic levels would become negligible, and at high excitation similar level densities would be approached. If such is the case, it would be expected that magic number and odd-even effects would be felt principally in the last evaporation step, and to a decreasing extent in the preceding evaporation steps where the excitation energy is higher. Thus, if it were possible to observe the  $\text{Co}^{59}(p,6n)\text{Ni}^{54}$  reaction, we might expect to find its cross section not as strongly reduced compared to the corresponding copper reaction as that of the doubly magic  $\text{Ni}^{56}$ , although the former reaction must pass through an excited state of  $\text{Ni}^{56}$ . Such behavior has been observed in a series of odd-odd and even-even nuclei reactions.

#### D. Total Absorption Cross Section

Rudstam<sup>4</sup> has shown that the spallation yields for 187-Mev protons on vanadium, manganese, and cobalt can be represented by parabolic plots of yield  $vs$   $Z$  for each mass number. A similar plot has been made for the 100-Mev spallation yields obtained in this study, where the yield as a function of  $A_p - A_0$  is plotted for all the observed products below nickel [Fig. 9(a)].  $A_p - A_0$  represents the distance of the product  $A_p$  from the nuclide of maximum yield  $A_0$ , where  $A_0$  was chosen as suggested by Le Couteur<sup>44</sup> to be one half-unit on the

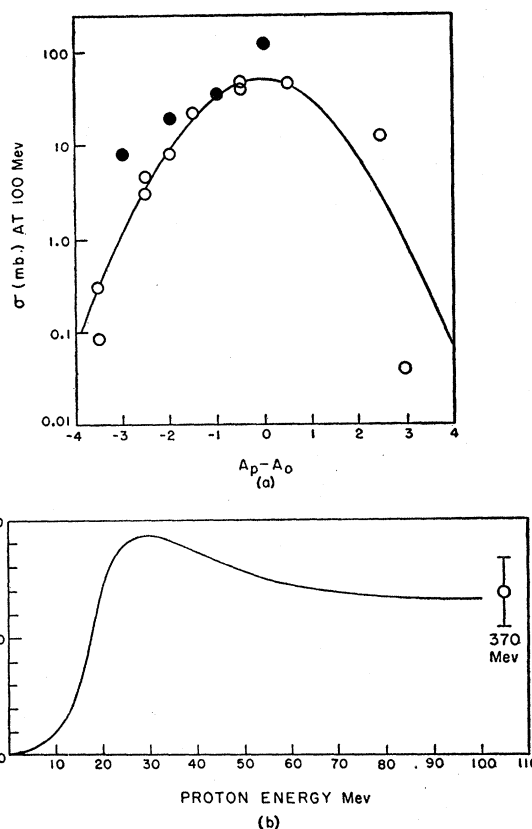


Fig. 9. (a) Cross section  $vs$  displacement from mass surface valley:  $\bullet$  Co isotopes;  $\circ$  others. (b) Absorption cross section  $vs$  energy.

neutron deficient side of stability. The yields fall pretty well on the parabola  $\log \sigma = 1.7 - 0.175(A_p - A_0)^2$ ; this sharp decrease in yield with distance from the stable valley is further strong evidence for the important role of the evaporation mechanism which strongly favors de-excitation modes leading towards the stable valley.

By using the excitation functions in this study, a series of curves similar to Fig. 9(a) were constructed at five-Mev intervals from which were obtained the yields of all nuclides from the elements vanadium through cobalt. Yields at each energy interval were then summed and a plot made of the total absorption cross-section  $\sigma$   $vs$  energy [Fig. 9(b)]. Yields of the magic number nuclides  $\text{Ni}^{58}$  and  $\text{Ni}^{59}$  were assumed to be depressed fivefold compared to the same reactions in copper and the yield of the proton inelastic scattering reaction  $(p,p')$  was ignored. These approximations may both lead to underestimation of  $\sigma$  below 20 Mev. Neglecting contributions to the total absorption cross sections from products below vanadium, as estimated from Rudstam's yields<sup>4</sup> and Wagner and Wiig's excitation functions,<sup>2,3</sup> causes errors of about 5% at 100 Mev.

While a plot of this kind does not yield precise information and also smooths out irregularities due to

<sup>42</sup> Hughes, Garth, and Levin, Phys. Rev. **91**, 1423 (1953).

<sup>43</sup> H. Hurwitz and H. A. Bethe, Phys. Rev. **81**, 898 (1951).

<sup>44</sup> K. J. Le Couteur, Proc. Phys. Soc. (London) **A63**, 259 (1950).

heavy-particle emission, the trend of the result is clear. At energies of 20–30 Mev where the compound nucleus picture is most valid the nucleus appears blackest and shows an absorption about equal to the geometrical cross section of 1.00 barn. Extrapolating the flat portion of the curves to 370 Mev shows agreement with the total absorption cross section at that energy estimated by Belmont and Miller,<sup>1</sup> while the 685-mb value at 90 Mev compares favorably with the 730-mb inelastic cross section for 90-Mev neutrons on copper measured by Hadley and York.<sup>23</sup>

#### V. ACKNOWLEDGMENTS

The authors owe particular thanks to Dr. James W. Meadows for his continued help with the experiments and for many fruitful discussions. The cooperation of the staff of the Harvard 95-in. cyclotron is also gratefully acknowledged. The Berkeley linear-accelerator bombardments would not have been possible without the generous assistance of Dr. E. K. Hyde of the Radiation Laboratories. Thanks are also due to Professor J. W. Irvine and Dr. P. J. Kafalas for several cyclotron-produced tracers used in this work.

### Gamma-Ray Angular Distribution in Coulomb Excitation\*

G. BREIT, M. E. EBEL, AND J. E. RUSSELL  
Yale University, New Haven, Connecticut

(Received October 31, 1955)

In view of discrepancies in the literature regarding signs in formulas for the angular distribution of gamma rays emitted in Coulomb excitation, this distribution is worked out for the special case of  $0 \rightarrow 2$  transitions. The calculation is quantum mechanical and neglects higher than first-order effects in the Coulomb energy. The signs and forms obtained are confirmed by a semiclassical calculation.

CONSIDERABLE interest has recently been attached to the angular distribution of gamma rays from nuclear states excited by the Coulomb field of impinging particles. The angular correlation in question is between the direction of the incident particle and that of the gamma emitted in de-excitation. The original work of Alder and Winther<sup>1</sup> pointed out the possibilities of the subject and gave correctly the relative signs of the contributions to the coefficients of the Legendre functions in their formula. In their numerical application however, some of these signs appear to have been incorrectly used. This applies to the sign of the term multiplying  $P_4$  as a whole in their formula as well. In the work of Biedenharn and Class<sup>2</sup> some relative signs in the term multiplying  $P_2$  are incorrect, agreeing with Alder and Winther's arithmetic rather than their formula. Since the general formalism used by Biedenharn and Class requires minute attention regarding conventions of notation it appears desirable to outline a short calculation of these coefficients, which while not covering the most general case suffices for ascertaining all factors in the general formula with the exception of providing the general interpretation of the nuclear quadrupole matrix element. It thus determines the signs of the terms giving the coefficients  $a_2(\xi)$  in the quantum generalization of the Alder-Winther formula.

In this the interaction between the field of the incident particle and the multipole moment of the nucleus, and that between the nucleus and the radiation field are treated as perturbations; the Coulomb term of the interaction between nucleus and incident particle is treated exactly, however. The particular calculation has assumed excitation of a nucleus originally in a  $J=0$  state to a  $J=2$  state, and the subsequent  $\gamma$  decay of the nucleus back to a  $J=0$  state. The two steps involved in the process are thus, first, the Coulomb excitation to one of these  $J=2$  nuclear sublevels, and, secondly, the radiative transition from the sublevel to the ground state. Each sublevel gives rise to a characteristic distribution of radiation; the anisotropy of the  $\gamma$  distribution is due to the various sublevels being excited with different amplitudes.

The intensity of the  $\gamma$  emission is proportional to the square of the absolute value of the matrix element of the interaction energy for this process. This matrix element in turn is proportional to the sum over sublevels of the product of the amplitude for excitation of a given sublevel and the amplitude of the radiation emitted in a given direction in the de-excitation of this level. Here it is assumed that the sublevels are part of a degenerate level. Since the polarization of the gamma ray is not observed, the intensities arising from the two possible polarizations of the radiation are added. The angular correlation being the only quantity of interest here, only the dependence of the excitation amplitude on the magnetic quantum number  $\mu$ , and the dependence of the radiation amplitude upon  $\mu$  and the direction of emission

\* This research was supported by the United States Air Force, through the Office of Scientific Research of the Air Research and Development Command.

<sup>1</sup> K. Alder and A. Winther, *Phys. Rev.* **91**, 1578 (1953).

<sup>2</sup> L. C. Biedenharn and C. M. Class, *Phys. Rev.* **98**, 691 (1955).